JGR Oceans

RESEARCH ARTICLE
10.1029/2018JC014624

Special Section:
Forum for Arctic Modeling and Observational Synthesis (FAMOS) 2: Beaufort Gyre phenomenon

Critical Role of Continental Slopes in Halocline and Eddy Dynamics of the Ekman-Driven Beaufort Gyre

G. E. Manucharyan[1] and **P. E. Isachsen**[2,3]

[1]Environmental Science and Engineering, California Institute of Technology, Pasadena, CA, USA, [2]Department of Geosciences, University of Oslo, Oslo, Norway, [3]Norwegian Meteorological Institute, Oslo, Norway

Key Points:
- Beaufort Gyre halocline and eddy dynamics are affected by continental slopes
- Eddy momentum fluxes over the slopes counteract the Ekman component of the overturning and reduce eddy diffusivity
- As a consequence of reduced eddy diffusivity over slopes, the halocline deepens and has a prolonged equilibration timescale

Correspondence to:
G. E. Manucharyan,
gmanuch@uw.edu

Citation:
Manucharyan, G. E., & Isachsen, P. E. (2019). Critical role of continental slopes in halocline and eddy dynamics of the Ekman-driven Beaufort Gyre. *Journal of Geophysical Research: Oceans*, *124*, 2679–2696. https://doi.org/10.1029/2018JC014624

Received 1 OCT 2018
Accepted 26 FEB 2019
Accepted article online 12 MAR 2019
Published online 16 APR 2019

Abstract The Beaufort Gyre (BG) is a large-scale bathymetrically constrained circulation driven by a surface Ekman convergence that creates a bowl-shaped halocline and stores a significant portion of the Arctic Ocean's freshwater. Theoretical studies suggest that in the gyre interior, the halocline is equilibrated by a balance between Ekman pumping and counteracting mesoscale eddy transport energized by baroclinic instability. However, the strongest anticyclonic flows occur over steep continental slopes, and, despite bathymetric slopes being known to influence baroclinic instability, their large-scale impacts on BG halocline remain unexplored. Here we use an idealized eddy-resolving BG model to demonstrate that the existence of continental slopes dramatically affects key gyre characteristics leading to deeper halocline, stronger anticyclonic circulation, and prolonged equilibration. Over continental slopes, the magnitude of the Eulerian mean circulation is dramatically reduced due to the Ekman overturning being compensated by the eddy momentum-driven overturning. The eddy thickness flux overturning associated with lateral salt transport is also weakened over the slopes, indicating a reduction of eddy thickness diffusivity despite the isopycnal slopes being largest there. Using a theoretical halocline model, we demonstrate that it is the localized reduction in eddy diffusivity over continental slopes that is critical in explaining the halocline deepening and prolonged equilibration time. Our results emphasize the need for observational studies of eddy overturning dynamics over continental slopes and the development of slope-aware mesoscale eddy parameterizations for low-resolution climate models.

1. Introduction

The Beaufort Gyre (BG) is a large-scale anticyclonic circulation feature in the Arctic Ocean's Canadian Basin that stores a substantial amount of freshwater. The freshwater budget depends on the balance of precipitation/evaporation/runoff and the salinity flux from inflowing/outflowing waters (Haine et al., 2015). The BG circulation is largely maintained by wind- and ice-induced surface ocean stresses (Proshutinsky et al., 2002, 2009). The winds over the Canada Basin vary strongly on seasonal and longer timescales but are on average anticyclonic, causing Ekman convergence in the interior of the basin, halocline deepening, and corresponding anticyclonic geostrophic currents. The stress transfer is modulated by sea ice motion, but the annual mean effect is still a net surface Ekman convergence (Dewey et al., 2018; Meneghello et al., 2018a; Zhong et al., 2018).

The BG freshwater content (FWC), a linear metric of the amount of salt (or lack thereof) in the gyre, also undergoes significant changes on seasonal, interannual, and longer timescales (Giles et al., 2012; Haine et al., 2015). In situ ocean observations demonstrate an about 30% increase in FWC in the period 2003–2008, after which the increase has slowed down with an occurrence of a significant FWC drop in 2013 followed by its quick recovery in the following years (Beaufort Gyre Exploration Project, 2019). Understanding FWC variability remains a major challenge as the development and validation of theoretical models is inhibited by the lack of eddy-resolving Arctic Ocean simulations and comprehensive long-term observations.

1.1. BG Equilibration

Our basic understanding of the BG halocline evolution revolves around the ideas of Proshutinsky et al. (2002) with the gyre viewed as a flywheel driven by Ekman pumping due to the anticyclonic surface stress. The halocline deepens when there is Ekman pumping and shallows when there is Ekman suction, that is, $h_t = w_{\mathrm{Ek}}$, where h is a bulk measure of halocline depth (the subscript t indicates a time derivative) and w_{Ek} is the amplitude of the Ekman pumping. However, within this basic paradigm, a steady state cannot be achieved

for any nonzero time-mean Ekman pumping, and thus, a stabilizing process must exist to counteract the Ekman-driven halocline deepening. Near its stable equilibrium, the halocline evolution under relatively small perturbations obeys $h_t = w_{\mathrm{Ek}} - h/T_{\mathrm{eq}}$, where $T_{\mathrm{eq}} > 0$ is a halocline equilibration timescale, as introduced in Manucharyan and Spall (2016) and Manucharyan et al. (2016). Note that T_{eq} is an equilibrium state characteristic, and hence, it could change if halocline depth perturbations are sufficiently large for the omitted nonlinearities to become significant. Nonetheless, considering relatively small gyre deviations from equilibrium, the halocline depth perturbation in response to a persistent anomaly in Ekman pumping is determined by a product of the forcing and the equilibration timescale, that is, $h = T_{\mathrm{eq}} \cdot w_{\mathrm{Ek}}$. For time-varying forcing, the amplitude of halocline depth fluctuations decreases rapidly with the Ekman pumping frequency (Manucharyan et al., 2016). Thus, in order to understand and accurately model halocline depth variations, it is not only necessary to quantify external forcing but also to identify critical mechanisms responsible for internal gyre equilibration.

The equilibration timescale is an intrinsic gyre characteristic quantifying the efficiency of the stabilizing mechanisms. It could be diagnosed by exploring the temporal gyre evolution, either by conducting forced perturbation experiments (Marshall et al., 2017) or by observing halocline fluctuations in long simulations with naturally varying forcing (Johnson et al., 2018). Across a range of low-resolution climate models participating in the BG "Climate Response Functions" coordinated experiments (Marshall et al., 2017) the diagnosed equilibration timescales range from interannual to decadal, indicating a disagreement in the way models represent gyre equilibration processes.

Hypotheses about the BG equilibration processes, among others, include (i) halocline flattening due to mesoscale eddies formed via baroclinic instability in order to release the available gravitational potential energy (APE) stored in a bowl-shape halocline (Manucharyan & Spall, 2016), (ii) frictional dissipation of its geostrophic currents by rubbing against the sea ice (Dewey et al., 2018; Meneghello et al., 2018a; Zhong et al., 2018), and (iii) a balance between vertical diffusion in the interior of the gyre and eddy fluxes from its boundaries (Spall, 2013). The vertical mixing hypothesis does not rely on the intensity of Ekman pumping and hence can only provide a partial explanation of the dynamics. The ice friction mechanism, also referred to as the *Ice Governor* (Meneghello et al., 2018b), relies on the presence of sea ice that reduces the surface ocean stress (and hence reduces the Ekman pumping) when geostrophic currents develop. However, the BG is already seasonally ice covered and in the limit of complete sea ice disappearance other equilibration mechanisms must take over. Although all of the mentioned hypotheses may be contributing to BG equilibration, in this idealized study, we will focus on the eddy hypothesis (i) as mesoscale eddies are expected to form in the Arctic regardless of vertical mixing or the presence of sea ice as long as there are sufficiently strong baroclinic currents.

1.2. Role of Eddies in Halocline Dynamics

Using a mesoscale eddy-resolving model, Manucharyan and Spall (2016) demonstrated that a realistic BG halocline can indeed support sufficient mesoscale eddy transport to counter the Ekman pumping. The halocline depth as well as the FWC equilibration timescale are inversely proportional to the mesoscale eddy diffusivity in these idealized studies, that is, $h \sim R\tau(\rho_0 f K)^{-1}$ and $T_{\mathrm{eq}} \sim R^2 K^{-1}$, where τ is the anticyclonic surface stress, R is the gyre radius, and K is the Gent-McWilliams (GM) eddy thickness diffusivity (Gent & Mcwilliams, 1990; Gent et al., 1995), which may depend on the flow field itself. Equilibration occurs when the information about the forcing and boundary conditions is propagated across the gyre via eddy diffusion of halocline thickness (Manucharyan et al., 2016). Since the halocline evolution is governed by a diffusion equation, any local variations in the eddy diffusivity will have global impacts on halocline shape and equilibration timescale.

Eddy diffusivity in the BG can vary significantly depending on the mean flow, stratification and as we will demonstrate in this study, continental slopes. Observational evidence from mooring data suggest that eddy diffusivity reaches values of about 600 m^2/s (Meneghello et al., 2017), which is sufficient to counteract the Ekman pumping of about 10 m/year given the observed magnitudes of the halocline slopes. In the idealized eddy-resolving model of Manucharyan and Spall (2016), which is characterized by a balance between eddy transport and Ekman pumping, an eddy diffusivity of 300 ± 200 m^2/s were diagnosed, with higher values near gyre boundaries that have large halocline slopes. However, all these idealized simulations, as well as the mooring locations, are over a flat-bottom basin, whereas the real gyre has a complicated bathymetry with continental slopes extending 20–200 km away from the shelf break (Figure 1). Since typical halocline

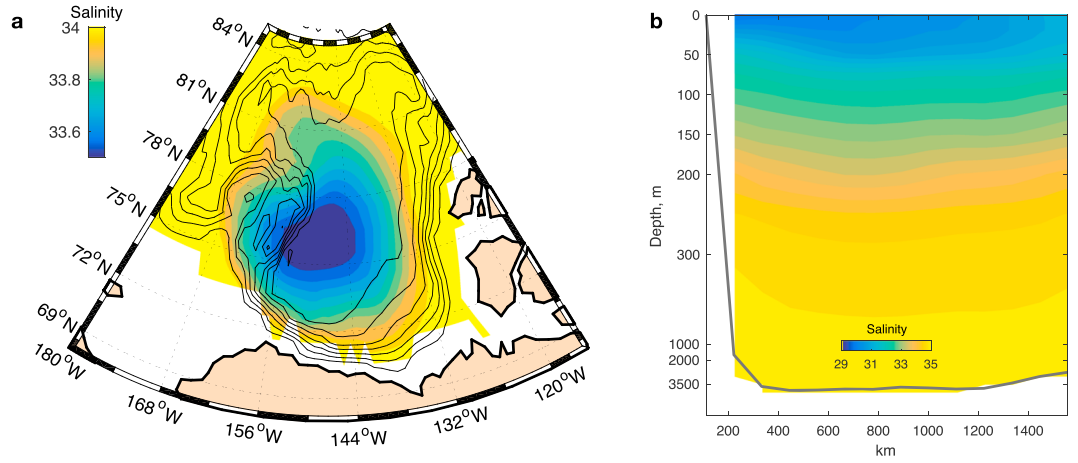

Figure 1. (a) Annual mean Beaufort Gyre salinity at 200-m depth (colors) and isobaths at 500-m intervals (black lines). Salinity data come from the Polar Science Center Hydrographic Climatology (Steele et al., 2001). Note that the gyre is to a large degree constrained by the surrounding topography including steep continental slopes that are directed in the same sense as the halocline slopes. (b) Salinity transect passing through the gyre center along a constant longitude of 150°W (color), and gray line denotes bathymetry; vertical axis below 500 m has been squeezed by a factor of 50 to emphasize upper-ocean halocline features.

slopes are of the order of 100 m/500 km = 0.002, significantly smaller than the steepness of the continental slopes, the stability of the geostrophic currents and associated eddy properties can be greatly affected.

1.3. Topographic Influence on Baroclinic Instability and Eddies

What is known about topographic influence on baroclinic instability comes primarily from modified Eady (1949) or two-layer Phillips (1954) theory in which the inclusion of a linearly sloping bottom still allows for analytic solutions (Blumsack & Gierasch, 1972; Brink, 2012; Isachsen, 2011; Mechoso, 1980). Much of the qualitative behavior can be understood from how the bottom steers the trajectories of fluctuating water parcels (and hence the eddy buoyancy flux) in relation to the "wedge of instability." Essentially, APE is released if the eddy buoyancy flux is inclined somewhere between the horizontal and the slope of the isopycnals (Mechoso, 1980). A maximum APE release takes place when the slope of the buoyancy flux is half that of the isopycnals (Pedlosky, 1982; Visbeck et al., 1996). Hence, in the modified Eady model, the effect of the bathymetry on the steering of water parcels is represented by a parameter $\delta = s_b/s$ measuring the ratio of the bottom slope, s_b, to the isopycnal slope, s.

The response is asymmetric with respect to the sign of δ. For $\delta < 0$, the situation in which isopycnal and bottom slope have opposite signs (as for a buoyant surface current flowing with the coast to its right in the Northern Hemisphere), the bottom is forcing deep water parcels to move outside of the wedge of instability. Instability is still possible since parcels higher up in the water column are able to follow trajectories that fall within the unstable wedge. But both growth rates and associated length scales reduce monotonically with steeper (negative) bottom slopes. For $\delta > 0$, the situation is more complex. For $0 < \delta < 1$, the bottom actually guides the eddy fluxes to be within the wedge of instability and growth rates attain maximum values for $\delta = 0.5$. But for $\delta > 1$, growth shuts off completely. This shutoff cannot be understood from kinematic arguments alone (since parcels would be free to move within the unstable wedge away from the bottom). The shutoff for steep bottom slopes must instead be understood from dynamic arguments, most easily illustrated in the two-layer Phillips framework: When the topographic slope is larger than the isopycnal slope, the horizontal potential vorticity (PV) gradient does not change sign between the layers—a necessary condition for instability.

The BG is in the $\delta > 1$ regime as topographic slopes are in the same direction as isopycnal slopes but stronger (Figure 1). Thus, over continental slopes, the currents should be baroclinically stable according to modified Eady or Phillips theory. But this is in apparent contradiction with observations of an energetic eddy field around the slopes. One possibility is that baroclinic instability of the halocline layer does not occur over the slopes, and the observed eddies are generated elsewhere or by other processes, for example, stemming from instabilities of the shelf break current flowing cyclonically around the Arctic basins (Aksenov et al., 2011),

from mixed layer instabilities or any higher baroclinic mode instabilities occurring over the entire basin. However, note that a mere presence of eddies is not sufficient to generate down-gradient eddy thickness fluxes, which necessarily occur during local baroclinic instability. Thus, it is not clear if isolated eddies that have propagated into the gyre interior can generate thickness fluxes to counteract the Ekman pumping there. Another possibility is that the gyre is still baroclinically unstable over the slopes but due to dynamics that is not captured by the extremely simplified Eady or two-layer Phillips theories. This is the hypothesis that we follow in this study.

Since the gyre equilibration timescale and halocline depth are directly dependent on eddy diffusivities (Manucharyan et al., 2016), continental slopes would have a global impact if they indeed affect the eddy field. However, climate models, including those participating in Coupled Model Intercomparison Projects or in BG "Climate Response Functions" studies do not resolve eddy dynamics over continental slopes and do not have any slope-aware eddy parameterizations, which may lead to their misrepresentation of halocline equilibration processes. Motivated by these shortcomings, we here present a set of idealized simulations addressing the issue of gyre equilibration and eddy dynamics in the presence of continental slopes.

1.4. Manuscript Outline

In section 2, we offer a brief review of the representation of eddies in the so-called transformed Eulerian mean (TEM) framework of Andrews and McIntyre (1976), a perspective that has proved invaluable in analyzing the integrated effects of turbulent atmospheric and oceanic flows. In section 3, we present our idealized model setup and sensitivity experiments. In section 4, we begin to present results by showing key halocline characteristics that are affected by the inclusion of continental slopes. In section 5, we then look more closely at how eddies transport buoyancy and momentum, keeping our focus on the impact of continental slopes. In section 6, we present an eigenvalue analysis of a halocline evolution model that explains the reasons behind global impacts of continental slopes on the BG equilibration timescale and FWC. A summary and final discussions of results are given in section 7.

2. Background: BG Overturning in the TEM Framework

The TEM framework (Andrews & McIntyre, 1976) allows one to illuminate the role of eddy fluxes in the evolution budgets of large-scale mean momentum and tracer fields. The mean we will be using in this manuscript refers to an azimuthal mean around a closed ocean gyre.

2.1. Eddy Streamfunction and Diffusivity

In our simulations salinity controls buoyancy. In the absence of diabatic sources and sinks as well as small-scale diabatic mixing, the evolution of the azimuthal mean salinity, $\bar{S}$, is affected by the mean flow advection as well as vertical and horizontal eddy salinity fluxes:

$$\bar{S}_t + \bar{v}\bar{S}_r + \bar{w}\bar{S}_z + \overline{v'S'}_r + \overline{w'S'}_z = 0, \tag{1}$$

$$\bar{v} = -\bar{\psi}_z, \quad \bar{w} = \frac{1}{r}(r\bar{\psi})_r. \tag{2}$$

Here bars and primes correspond to mean and perturbation (or eddy) variables, and $\bar{v}$ and $\bar{w}$ are radial and vertical components of an incompressible mean flow in the (r, z) plane defined by the Eulerian mean overturning stream function, $\bar{\psi}(r, z, t)$.

Making use of the near-adiabatic nature of mesoscale eddies (that is, eddy salt fluxes are nearly perpendicular to the mean salinity gradient, $\overline{v'S'}_r/\overline{w'S'}_z \simeq -\bar{S}_z/\bar{S}_r$), the eddy salt flux divergence can be represented as an additional advection:

$$\bar{S}_t + (\bar{v} + v^*)\bar{S}_r + (\bar{w} + w^*)\bar{S}_z = 0, \tag{3}$$

where the nondivergent eddy velocities v^* and w^* are defined by an eddy "thickness flux" stream function ψ^* such that

$$\psi^* = \frac{\overline{v'S'}}{\bar{S}_z} = -\frac{\overline{w'S'}}{\bar{S}_r}. \tag{4}$$

Essentially, when salinity controls buoyancy (as we specify here) ψ^* represents the cumulative effects of eddy thickness fluxes that arise from correlations between eddy velocities and eddy isopycnal displacements.

Ocean models that do not resolve mesoscale eddies must parameterize the eddy stream function. They commonly do so according to the GM parameterization (Gent & Mcwilliams, 1990; Gent et al., 1995) where the horizontal component of eddy buoyancy fluxes are assumed to be down-gradient, that is, $\overline{v'S'} = -K\bar{S}_r$ so that $\psi^* = Ks$, where K is an eddy diffusivity and s is the isopycnal slope. The original GM parameterization does not specify how to prescribe K and climate modelers need to make further assumptions, for example, use a spatially homogeneous diffusivity or prescribe it to be a linear function of the bulk isopycnal slope (Visbeck et al., 1997). Identifying a closure for eddy diffusivity in terms of mean state variables remains a major theoretical challenge.

2.2. Eulerian Mean and Residual Overturning

The Eulerian mean stream function, $\bar{\psi}$, can also be affected eddies, but in this case by eddy momentum fluxes that enter the evolution equation for the mean azimuthal flow. Assuming flow on an f plane (a good approximation for the BG), we have

$$\bar{u}_t + \overline{(v'u')}_r + f\bar{v} = \bar{\tau}_z/\rho_0, \tag{5}$$

where u is the azimuthal flow (positive for cyclonic direction) and v is the radial flow (positive away from gyre center), f is the Coriolis parameter, and $\bar{\tau}(r,t)$ is the mean kinematic stress in the azimuthal direction. We have neglected minor contributions from the azimuthal mean flow advection and the vertical eddy transport of azimuthal momentum. Since $\bar{v} = -\bar{\psi}_z$, we can integrate the momentum equation vertically from the surface where stress is externally defined to any depth z outside the Ekman layers where the stress is negligible. In steady state, the Eulerian mean stream function in the interior of the ocean is then governed by the surface stress and the vertical integral of the eddy momentum flux convergence:

$$\underbrace{\overline{\psi}(r,z)}_{\text{Eulerian mean}} = \underbrace{\left.\frac{\bar{\tau}}{\rho_0 f}\right|_{z=0}}_{\text{Ekman-driven: } \psi_{\text{Ek}}} \underbrace{-\frac{1}{f}\int_z^0 \overline{(u'v')}_r \mathrm{d}z}_{\text{Eddy momentum-driven: } \psi_{\text{em}}} . \tag{6}$$

For large-scale oceanic flows, the surface-stress-driven (Ekman) stream function, ψ_{Ek}, is typically considered dominant while the eddy momentum-driven stream function, ψ_{em}, is commonly ignored, for example, in the Antarctic Circumpolar Current models (Marshall & Radko, 2003) or in the interior of the BG (Manucharyan & Spall, 2016). Nonetheless, a clear example of an eddy momentum-driven overturning exist in the atmosphere in the form of the Ferrel cell (Schneider, 2006). In addition, strong lateral current shears caused by, for example, topography may develop an anisotropic eddy field (Hoskins et al., 1983), which provides significant changes to the Eulerian stream function from the purely surface stress-driven component (see, for example, Wang & Stewart, 2018). In this manuscript, we will demonstrate that ψ_{em} is critically important near continental slopes of the BG and that it causes leading-order changes in the halocline depth and the gyre equilibration timescale.

The *residual* overturning stream function, $\overline{\psi^*}$, which directly transports tracers between their sources and sinks, is the sum of the Eulerian mean and the eddy thickness flux stream functions:

$$\overline{\psi^*} = \bar{\psi} + \psi^*, \tag{7}$$

where $\bar{\psi}$ and ψ^* have been defined in equations (4) and (6). Here we explore an idealized model of the BG that has negligible vertical mixing and no surface buoyancy fluxes so that the steady state residual mean circulation must be negligible: $\overline{\psi^*} \approx 0$ (by equation (3)). Thus, the gyre equilibrates when a three-way balance is achieved between the stream functions driven by the Ekman pumping, the eddy momentum fluxes and the eddy thickness fluxes, that is, $\psi_{\text{Ek}} + \psi_{\text{em}} + \psi^* = 0$.

The problem may also be cast in terms of a TEM residual momentum equation in which eddy momentum and thickness fluxes are grouped together as the "Eliassen-Palm" flux (see, for example, Vallis, 2006; Wardle & Marshall, 2000). Under steady state, the divergence of this flux in the z-r plane drives, in part, the residual overturning (time-mean stresses also contribute). If quasi-geostrophic scaling applies, the divergence of the Eliassen-Palm flux is also equivalent to a PV flux. Here, however, we choose to group eddy momentum fluxes along with the mean momentum fluxes that together set the Eulerian mean stream function. Eddy thickness fluxes are then diagnosed separately, and we end up with the classical decomposition shown in equation (7).

3. Idealized BG Model With Continental Slopes

We include continental slopes into the idealized BG model that was previously used in Manucharyan et al. (2016) to demonstrate that the Ekman-driven BG halocline can be efficiently equilibrated by mesoscale eddies. Our goal is to quantify the impact of continental slopes on mesoscale eddy transport and interior halocline dynamics.

3.1. Numerical Model and Basin Geometry

The primitive equations are solved using the Massachusetts Institute of Technology general circulation model (Marshall et al., 1997a, 1997b) run in a hydrostatic configuration. We use a linear equation of state with only salinity contributing to the buoyancy (temperature has a minor impact for such strongly stratified flows at near-freezing temperatures). A 4-km horizontal grid resolution with 42 vertical levels is used to ensure that mesoscale eddies are resolved. Depending on the gyre location and on the presence of continental slopes, the model stratification (see below) gives internal Rossby deformation radii that range between 13 and 20 km, being similar in magnitude to the observed radii (Nurser & Bacon, 2014). Depending on the offshore extent of continental slopes, the model was integrated for 20–100 years to reach statistical equilibrium. Given characteristic eddy velocities, a relatively short time step of 300 s was necessary to ensure numerical stability. An even higher model resolution, although preferred, is not practical as equilibrium experiments are computationally expensive (order of 30K CPU hours per experiment), and the simulated eddy sizes are O(100 km). The lack of a planetary beta effect and weak dissipation result in a highly efficient inverse energy cascade that increases the equilibrium eddy size. These relatively large simulated eddies have the first baroclinic mode structure, being distinct from the O(10 km) higher baroclinic mode eddies detected by, for example, BG moorings (Zhao et al., 2018). Yet the salinity transport done by these large-scale eddies is sufficiently strong to arrest the halocline deepening at a depth comparable to observations. For a more comprehensive description of the model parameters, see Manucharyan and Spall (2016) and Appendix A therein. Continental slopes in our idealized BG extend linearly from a depth of 100 m to the bottom of the basin 3,500 m deep, with their offshore extent, L, being used as a sensitivity parameter. Vertical walls correspond to $L = 0$ and characteristic ranges for the BG is $L \sim$ (20–200 km) based on its bathymetric slopes of 0.01–0.1 (Figure 1). Thus, our idealized basin has a truncated cone shape with an interior depth of 3,500 m, a surface diameter of 1,200 km and a deep basin diameter ranging between 1,000 and 1,200 km depending on L. We conduct a set of sensitivity experiments varying the continental slope extent $L = [0, 25, 75, 100, 200]$ km.

3.2. Forcing: Surface Stress and Salinity Restoring

The model is driven by anticyclonic surface stress, which is 0 in the center and grows linearly toward the coast where it attains a maximum amplitude of $\tau_0 = 0.015$ N/m^2. This corresponds to a uniform Ekman pumping velocity of about 10 m/year. This is potentially an overestimate of Ekman pumping rates in light of new observational studies that incorporate satellite-derived surface geostrophic flow (Armitage et al., 2016) in calculations of the ocean surface stress (Dewey et al., 2018; Meneghello et al., 2018a; Zhong et al., 2018). However, our results do not qualitatively depend on the magnitude of the Ekman pumping, a sensitivity to which has been explored in detail in Manucharyan and Spall (2016) and Manucharyan et al. (2016); here we focus on highlighting the critical impacts brought by the inclusion of continental slopes.

The stratification is initialized with a horizontally homogeneous salinity distribution in a range between 29 and 34 salinity units to mimic the observed halocline. At the gyre boundaries, the salinity is strongly restored to a prescribed profile, which is the same as the initial halocline distribution. The strong restoring implies that effectively there is an infinite reservoir of freshwater, and hence, the halocline depth is only constrained by internal gyre dynamics and not by the freshwater availability. Another idealization that could be considered is an adiabatic gyre that does not have any salinity restoring. In this "no-restoring" case, the FWC can only be redistributed between different parts of the gyre—a limit perhaps most relevant on short timescales. In practice, the BG is somewhere in between the two idealized cases because its freshwater reservoir is limited by external processes such as precipitation/evaporation/runoff.

4. The Large-Scale Response to the Inclusion of Continental Slopes

The idealized BG spins up from the applied wind stress and eventually equilibrates to a state characterized by strong mesoscale eddy activity (Figure 2). The overall qualitative behavior is similar in simulations with

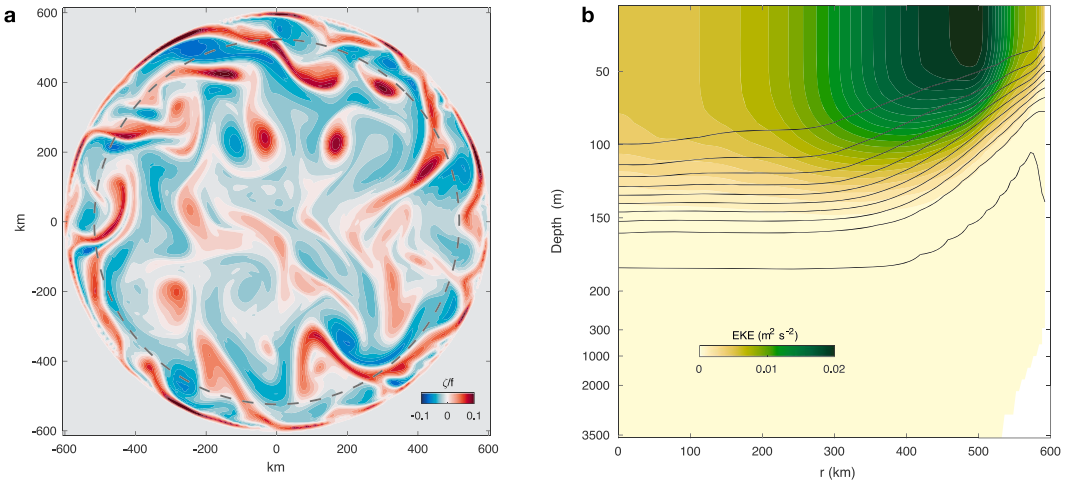

Figure 2. The equilibrated idealized Beaufort Gyre gyre. (a) Plan view snapshot of relative vorticity (normalized by Coriolis parameter f). The bathymetry includes continental slopes that extend 75 km offshore, linearly from 100 m to the bottom of the domain at 3,600 m; the maximum extent of the continental slope is indicated with a dashed line. (b) Azimuthal and time-mean eddy kinetic energy (EKE) density (colors) and corresponding salinity field (black lines) contoured at 0.5 intervals. The vertical coordinate below 250 m has been squeezed by a factor of 50 to emphasize deep ocean features. The continental slope is shown as a white patch in the bottom right corner.

vertical sidewalls and with continental slopes. However, as will be shown below, a number of key gyre characteristics are quantitatively affected by the presence of the slope: mainly the halocline depth, equilibration timescale, and the equilibrated overturning circulation.

4.1. Azimuthal Flow Field, FWC, and Equilibration Timescales

In simulations with a flat bottom and vertical side boundaries the halocline equilibrates at a depth of about 100 m (Figure 3a). The azimuthal flow field is anticyclonic with a maximum near the coast where the wind-stress magnitude is maximum, in line with linear Ekman-driven dynamics. The inclusion of continental slopes of width $L = 75$ km leads to an additional halocline deepening by about 40 m with the largest isopycnal steepening occurring in the vicinity of the slopes (Figure 3b). Associated with the steeper isopycnals over the continental slope is a strengthened and more spread-out anticyclonic mean flow and, in this particular case, the generation of a secondary surface velocity maximum where the continental slope meets the deep ocean. We also note a weak cyclonic flow at depth over the slope, a feature that is not present in the flat-bottom simulation. There is a qualitative similarity in the large-scale hydrography and azimuthal flow obtained in experiments with systematically changed width of continental slopes (Figure 4). In all simulations, we observe a near-linear FWC increase during the early stages, characteristic of linear Ekman-driven dynamics, followed by an exponential adjustment to equilibrium once eddies are formed (Figure 4a). For simulations with increasingly wider continental slopes, the equilibrium FWC is monotonically larger, ranging between 10×10^3 and 30×10^3 km^3. The corresponding surface azimuthal flow also increases from 0.1 to 0.5 m/s with increasing lateral extent of the continental slopes (Figure 4b), qualitatively consistent with idealized BG simulations in Lique et al. (2015) that only permitted the development of large eddies. The equilibration timescale, T_{eq}, diagnosed by fitting an exponential profile to the FWC spin-up time series, also increases with the extent of continental slopes, ranging from about 2 years for the slope-free gyre (vertical sidewalls) to over a decade for continental slopes extending 200 km offshore (Figure 4c). Using the equilibration timescale and the equilibrated FWC as scaling parameters, the FWC time series could be collapsed into a simple decaying exponential profile.

The observed linear relation between the equilibration timescale and equilibrated FWC (Figure 4c) conforms to theoretical predictions based on eigenvalue analysis of the halocline depth evolution equation (Manucharyan et al., 2016). Specifically, the equilibrium FWC change in response to Ekman pumping perturbations is directly proportional to T_{eq} and to the projection of the Ekman pumping perturbation onto the

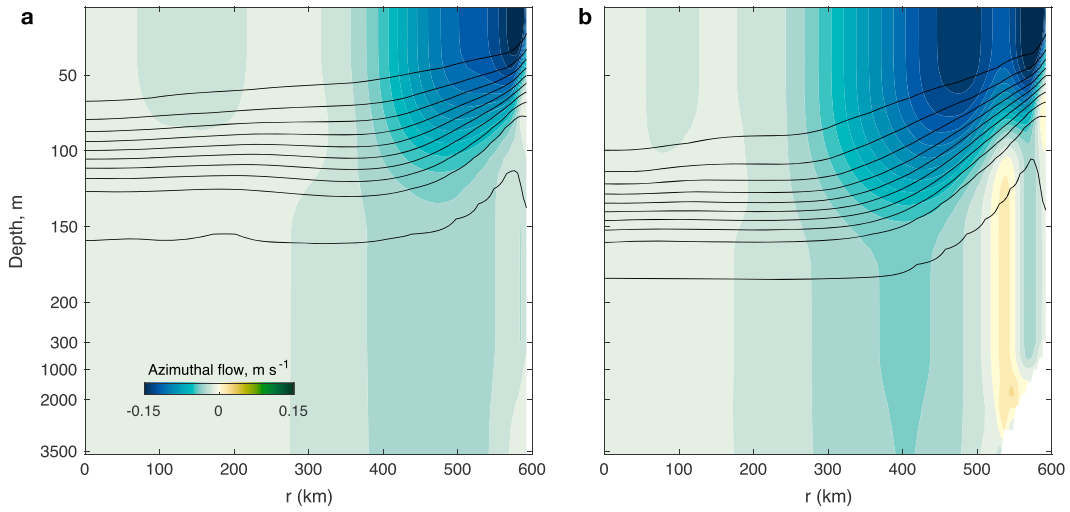

Figure 3. Equilibrated Ekman pumping-driven Beaufort Gyre state in simulations without continental slopes (a) and with continental slopes extending 75 km offshore (b). Colors show time-mean azimuthal flow (negative is anticyclonic), and black curves denote time-mean salinity contours at 0.5 intervals. The vertical coordinate below 250 m has been squeezed by a factor of 50 to emphasize deep ocean features. The continental slope is indicated by a white patch in the lower-right corner.

least-damped halocline eigenmode (see section 7 in Manucharyan et al., 2016). Changes in FWC, ΔFWC, in response to spatially uniform changes in Ekman pumping, Δw_{Ek}, can be expressed as

$$\Delta FWC = -T_{\mathrm{eq}}\ \Delta w_{\mathrm{Ek}}\ \left(A\frac{\delta S}{S_{\mathrm{ref}}}\right), \tag{8}$$

where A is the gyre area, δS is the cross halocline salinity difference, and S_{ref} is the reference salinity used in the calculation of the FWC; the minus sign appears because the Ekman pumping here is defined positive upwards and hence for anticyclonic stress w_{Ek} is negative while FWC is a positive quantity. While the above dependence was derived for a linear limit of small Ekman pumping perturbations, it can be used as a scaling law for explaining the equilibrium FWC from spin-up experiments by extending equation (8) to the nonlinear regime with $\Delta FWC \rightarrow FWC$ and $\Delta w_{\mathrm{Ek}} \rightarrow w_{\mathrm{Ek}}$. Indeed, the spin-up simulations demonstrate that the FWC sensitivity to the equilibration timescale is $2.7 \times 1,000\ \mathrm{km}^3$/year (Figure 4c), which is higher than the $1.9 \times 1,000\ \mathrm{km}^3$/year sensitivity predicted from equation (8) based on linear dynamics. The slight

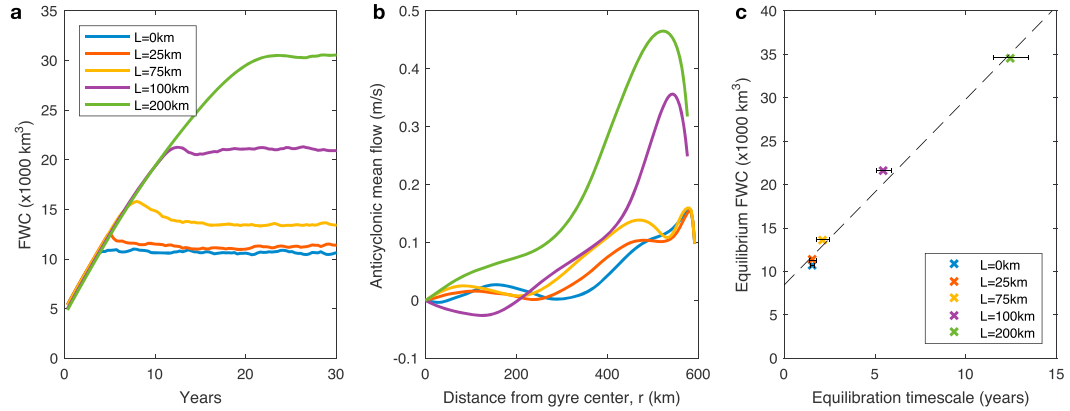

Figure 4. The large-scale response of the idealized Beaufort Gyre simulations for different continental slope widths. (a) Time evolution of the freshwater content (FWC). (b) Radial distribution of the surface anticyclonic mean flow. (c) FWC as a function of equilibration timescale (obtained by fitting an exponential law to the FWC time-evolution shown in panel a); the dashed line shows the best linear fit to data, and error bars reflect 95% confidence intervals for the equilibration timescale (FWC error bars are small and not shown). The widths the continental slopes are shown in the legend with colors consistent across the panels.

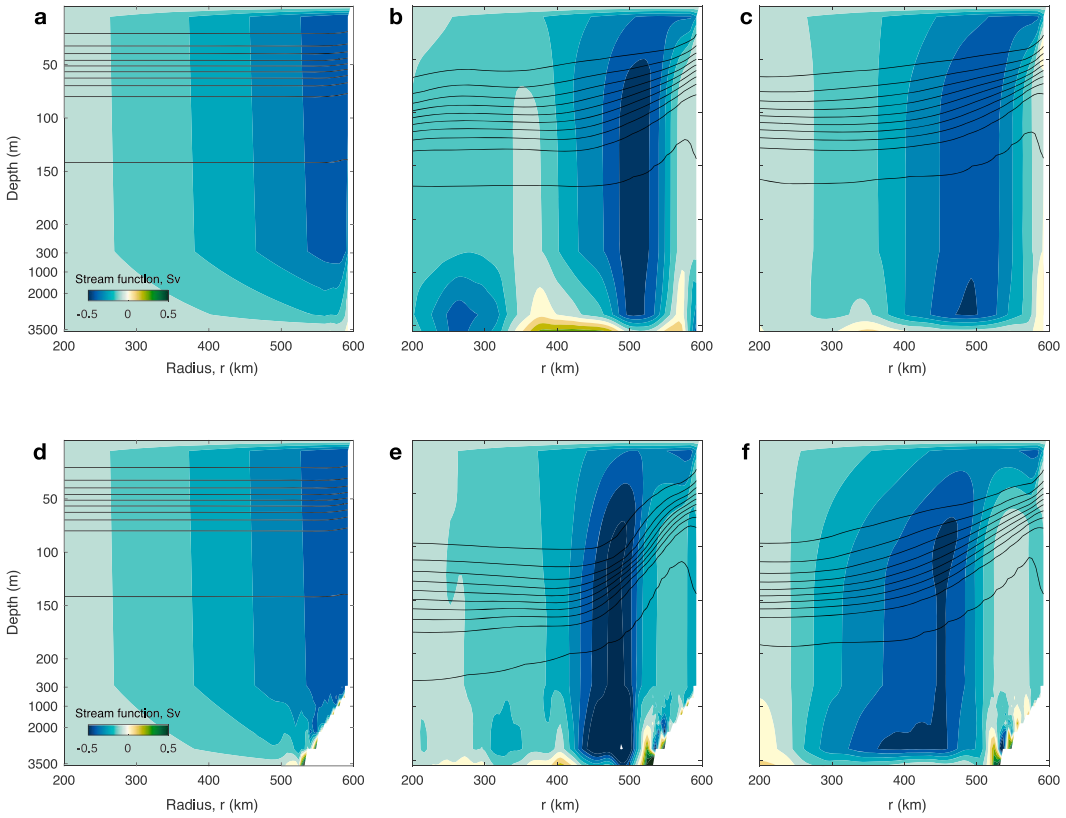

Figure 5. Time evolution of the Eulerian mean stream function in the (r, z) plane for a simulation without continental slopes (a–c) and with a continental slope extending 75 km away from the boundaries (d–f). (a, d) Stream functions in the beginning of the simulation in which the flow is dominated by the Ekman overturning, (b, e) at a stage where isopycnals are highly tilted and eddies just begin to form and (c, f) for a time-mean of the statistically equilibrated overturning with a fully developed eddy field. Negative and positive values indicate counterclockwise and clockwise circulation, respectively. The black curves are salinity contours equally spaced at 0.5 intervals. The fields are plotted starting 200 km from the center of the basin to emphasize processes over the continental slopes.

discrepancy in diagnosed and predicted sensitivities could be due to methodology biases in diagnosing T_{eq} from FWC spin-up time series as well due to limitations of applying equation (8) for large Ekman pumping perturbations. We will discuss a direct method for estimating the equilibration timescale as well as propose a path toward its parameterization in section 6.

Since the equilibration timescale in a slope-free gyre is inversely proportional to the characteristic eddy thickness diffusivity (Manucharyan & Spall, 2016), its dramatic increase for extended slopes suggests that a reduction of eddy diffusivity over continental slopes may be taking place. This behavior is consistent with an idea that steep bathymetric slopes suppress baroclinic instability. But the presence of eddies (Figure 2a) implies that instability is not completely inhibited as predicted for the $\delta > 1$ regime (topographic slope steeper than isopycnal slope) in modified Eady theory (Blumsack & Gierasch, 1972).

4.2. Eulerian Mean Overturning

The Eulerian mean overturning stream function, $\overline{\psi}(r, z)$, significantly changes in time during the spin-up processes, achieving a qualitatively distinct structure once the halocline deepens sufficiently to produce eddies (Figure 5). During the initial stage of spin-up, the Ekman-driven overturning dominates, that is, $\overline{\psi}(r, z) = \overline{\tau}(r)/(\rho_0 f)$; the downwelling is independent of depth outside the surface and bottom Ekman layers and the stream function increases linearly with radius with upwelling concentrated within O(10 km) from coastal boundaries (Figures 5a and 5d). However, once the eddy field is fully developed and the halocline reaches statistical equilibrium, the overturning has weakened over the continental slope by about an order of magnitude and nearly doubled in strength in the interior of the gyre right off the slope (Figures 5c and 5f). The weakening is qualitatively similar for the slope-free gyre but occurs only in a narrow vicinity of the coastal boundary (10–20 km in width). The inclusion of continental slopes, however, creates a *shadow zone*:

a region of nearly vanishing Eulerian mean stream function that extends across the entire continental slope. While the term is most commonly used in the ventilated thermocline theory to denote stagnant regions with no circulation (Luyten et al., 1983), the processes leading to such a region here are distinct. As we will discuss in section 5, the shadow zone here arises due to eddy momentum fluxes that drive an additional overturning that partially compensates the Ekman overturning. The dramatic departure of the Eulerian mean overturning from the Ekman pumping solution is inconsistent with the theoretical arguments of Manucharyan and Spall (2016) and Manucharyan et al. (2016) that ignore any eddy momentum contributions.

It is worth noting that a salinity tendency from mean advection arises only when streamlines of the Eulerian mean overturning are not aligned with isohalines (the advection term can be written as the Jacobian of the stream function and the salinity field). However, over the continental slopes, the Eulerian mean stream function at late stages in these simulations is more aligned with the isohalines compared to early stages during spin-up (Figure 5). This implies that the azimuthally averaged salinity tendency term (equation (3)) associated with mean advection is relatively small at late stages, and hence, the role for the eddy thickness flux overturning should also be reduced (to obtain a small residual circulation). Note that in the limiting case of the Eulerian mean circulation being perfectly aligned with isohalines there is no need for the eddy thickness flux overturning, and hence, the eddy thickness diffusivity should be zero.

5. Eddy Dynamics Over Continental Slopes

Mesoscale eddies predominantly form in regions where the mean anticyclonic flow is the strongest: either over continental slopes or near coastal boundaries if the gyre is slope free. These eddies are large-scale and deep. Because of the lack of surface buoyancy forcing, our idealized BG model does not generate a realistic mixed layer or any other isopycnal outcroppings, thus inhibiting the formation of higher baroclinic mode eddies—more energetic and localized eddies with peak velocities centered in the halocline that are commonly observed in BG moorings and Ice Tethered Profilers (Zhao et al., 2016, 2018). By construction, the cumulative salt transport by the modeled large-scale eddies must exactly counteract the Ekman transport and this balance leads to a realistic halocline depth of O(100 m). Below, we study the salt (buoyancy) and momentum transport made by the resolved eddy field.

5.1. Eddy Salinity Fluxes

In order to achieve an equilibrated salinity field in the adiabatic interior regions of our idealized BG gyre, any nonzero Eulerian mean overturning, $\overline{\psi}$, should be compensated by the eddy thickness flux stream function, ψ^* (see equation (3)). We diagnose this eddy stream function from lateral eddy salt fluxes, that is, from $\psi^* = \overline{v'S'}/\bar{S}_z$, where primes denote perturbations from the azimuthal mean and $\overline{v'S'}$ is the mean radial eddy salt transport (for a discussion of limitations of this method, see Plumb & Ferrari, 2005). Figure 6 shows both stream functions after spin-up. Perfect quantitative cancellation could not be achieved because we are estimating correlations in a very noisy eddy field. Nonetheless, a qualitative agreement and, to leading order, a quantitative compensation is evident. In fact, estimating the residual stream function directly (by diagnosing total volume transports in isopycnal layers, using the Massachusetts Institute of Technology general circulation model "Layers" package) revealed a residual overturning that was 1 to 2 orders of magnitude smaller than each of $\bar{\psi}$ and ψ^* (not shown).

The shadow zone in the Eulerian mean overturning over the continental slope is also present in the eddy thickness flux stream function (Figure 6b). This stems from a reduction in the eddy thickness diffusivity, as revealed by Figure 7a. Over the slopes, where the thermal wind shear is the strongest, the diffusivity is reduced by an order of magnitude compared to the interior of the gyre. So it is clear that the slopes suppress eddy buoyancy transport even if they do not shut down baroclinic instability completely (as would be predicted by the modified Eady theory of Blumsack & Gierasch, 1972). The same qualitative behavior is seen in all simulations, with the reduction being more severe for wide slopes (Figure 7b).

5.2. Eddy Momentum Fluxes

Before eddies have developed, the Eulerian mean stream function reflects only the linear Ekman-driven overturning ψ_{Ek}. But the stream function is substantially modified once the eddies are generated (Figure 5). The Ekman contribution to the Eulerian mean overturning has been discussed above, and here we focus on the eddy momentum-driven part, ψ_{em} (equation (6)). Eddies flux anticyclonic momentum offshore

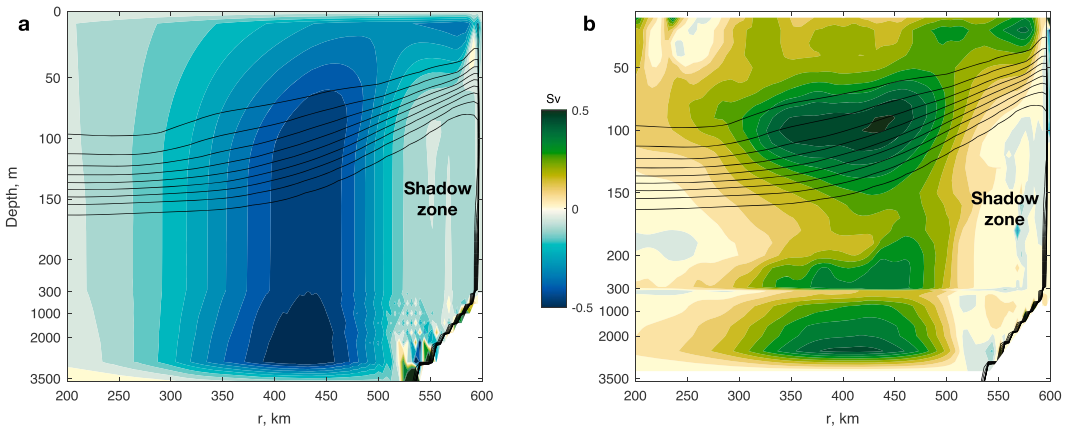

Figure 6. Eulerian mean stream function $\bar{\psi}$ (a) and thickness-weighted eddy stream function ψ^* (b) calculated for the equilibrated gyre. Note that the two stream functions appear to qualitatively compensate each other because the residual mean stream function, being the sum of the Eulerian mean and the eddy stream functions, must vanish as there are no significant buoyancy sources and sinks. Negative values indicate counterclockwise overturning; contours show time-mean isohalines at 0.5 intervals. The shadow zone over the continental slope denotes a region where both stream functions are dramatically weakened.

everywhere or, alternatively, flux cyclonic momentum toward the coast. As Figure 8 reveals, there is a strong eddy momentum flux convergence over the continental slope and a somewhat weaker but broader region of divergent fluxes offshore. As indicated by the TEM momentum equation (equation (5)), under nonequilibrium conditions, this pattern of flux convergence and divergence would tend to retard the anticyclonic flow over the slope and accelerate it offshore. In steady state, however, the Reynolds stresses are balanced by the Coriolis acceleration associated with the two counter-rotating overturning cells (shown in Figure 8b), one of which opposes the Ekman-driven steepening of the halocline over the continental slope. Note that the radial integral of ψ_{em} at any depth must be 0 due to the complete differential form of the integrand in equation (6). Due to this constraint, ψ_{em} must be changing sign in the interior of the gyre, which explains its counterrotating cells (Figure 8b).

The influence of eddies on the Eulerian mean overturning could also be estimated by taking a difference between the equilibrated Eulerian mean stream function and its value during the initial eddy-free stages of the spin-up. The temporal change in the Eulerian mean stream function is indeed quantitatively consistent with the eddy momentum-driven overturning diagnosed using equation (6) (compare Figures 8b and 8c).

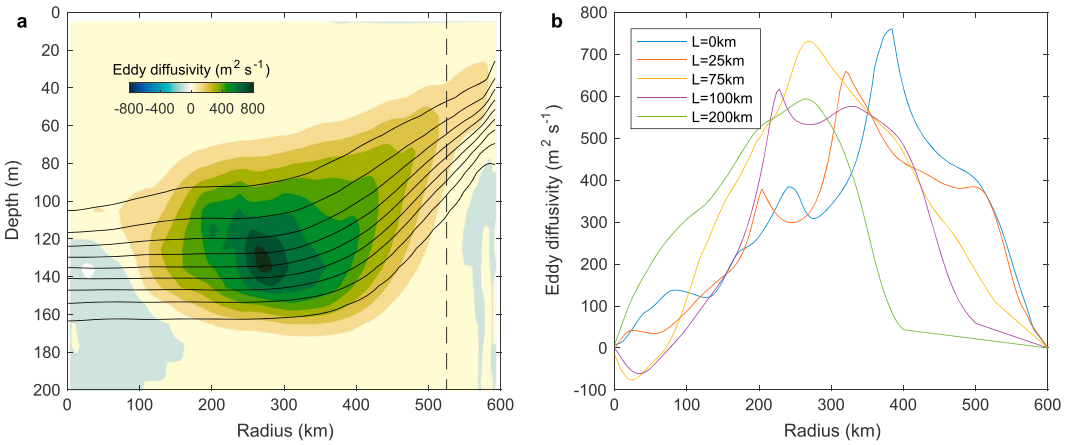

Figure 7. (a) Diagnosed eddy thickness diffusivity of a statistically equilibrated gyre with continental slopes of width 75 km; the vertical dashed line denotes the extent of the continental slope. **(b)** Radial dependence of the eddy diffusivity within the halocline for all simulations. Diffusivities have been tapered over the continental slopes, from a value right off the slope to 0 at the wall.

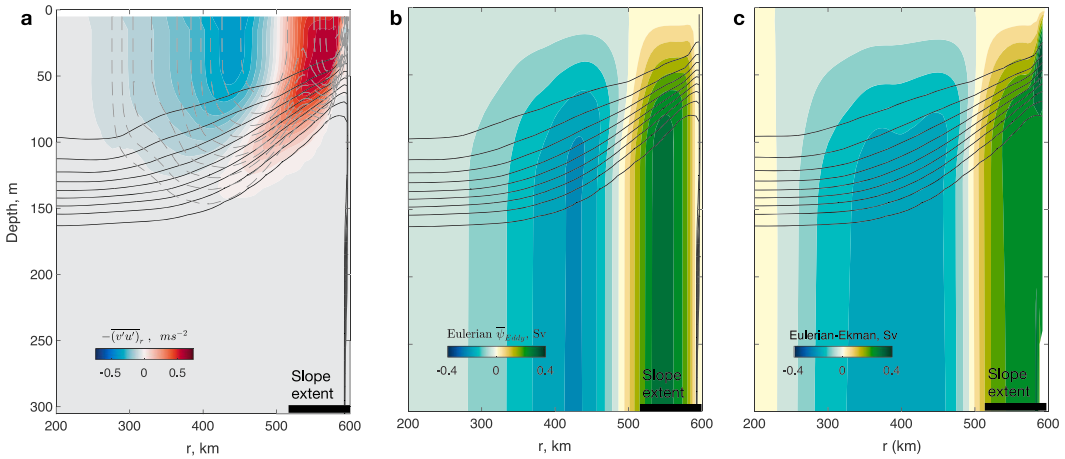

Figure 8. (a) Eddy momentum flux convergence. Positive values correspond to cyclonic tendencies (or a slowdown of the anticyclonic gyre circulation). Solid black lines show mean isohalines at 0.5 intervals, while dashed lines show the mean azimuthal velocity at 1-cm/s intervals. (b) Eddy momentum-driven stream function, ψ_{em}, calculated from the momentum flux convergence (equation (6)). (c) Eulerian mean overturning circulation in excess of Ekman overturning, diagnosed as a difference between the early stages of the spin-up where there are no eddies and the mean of the fully equilibrated gyre affected by eddies. Negative and positive values indicate counterclockwise and clockwise circulation, respectively.

The consistency between the two methods confirms that it is the eddy momentum fluxes that change the Eulerian mean flow and lead to shadow zones over continental zones.

5.3. Energy Conversion Rates

In order to explore the nature of eddy energy sources, we diagnose the barotropic and baroclinic energy conversion rates (e.g., Eden & Böning, 2002) defined as

$$C_{\mathrm{bt}} = -\overline{v'u'}\,\bar{u}_r, \quad C_{\mathrm{bc}} = -\overline{v'b'}\,\frac{\bar{b}_r}{\bar{b}_z}, \tag{9}$$

where buoyancy b depends linearly on salinity in these simulations. The barotropic conversion C_{bt} quantifies the transfer from mean kinetic energy (MKE) to eddy kinetic energy (EKE), thus acting as a local source term in the EKE density equation; EKE increases if eddies flux momentum down the mean radial velocity gradient—typically seen as a sign of barotropic instability. The baroclinic conversion C_{bc} quantifies the exchange between mean available potential energy (MAPE) and eddy available potential energy (EAPE); in this case, energy is extracted from the large-scale baroclinic flow (from the tilted density field) if lateral eddy buoyancy fluxes are down-gradient—a signature of baroclinic instability.

As seen above, the eddies bring anticyclonic momentum from the coast and into the basin causing a dipole pattern of convergence (Figure 8a). Considering the lateral gradients of the mean anticyclonic flow, the fluxes are down the gradient over the continental slope, out of the primary jet attached to the side boundary. They are then up the gradient right off the slope, feeding energy into the second jet found there, and are then finally down the gradient offshore of this second maximum (Figure 9a). Integrated over the entire domain there is therefore large cancellations, but the net effect is a small conversion of MKE to EKE. The two anticyclonic jets, in this view, are barotropically unstable on their offshore flanks. In contrast, the lateral buoyancy fluxes are down-gradient everywhere in the domain (Figure 9b). Thus, integrated over the basin the baroclinic conversion is much larger than the barotropic conversion, implying that baroclinic instability is the dominant process at play.

Consistent with the reduction of eddy thickness diffusivity observed over the continental slope (Figure 7c), baroclinic instability appears to be suppressed over the slope, and the MAPE-to-EAPE transfer is instead maximized over the flat-bottom interior of the gyre immediately offshore of the slope. In contrast, down-gradient eddy momentum fluxes, the signature of barotropic instability, are as large over the slope as anywhere else. Thus, in a global sense baroclinic instability emerges as the key process transferring the wind-induced momentum down (via eddy form stresses) and eventually to the ocean bottom where the

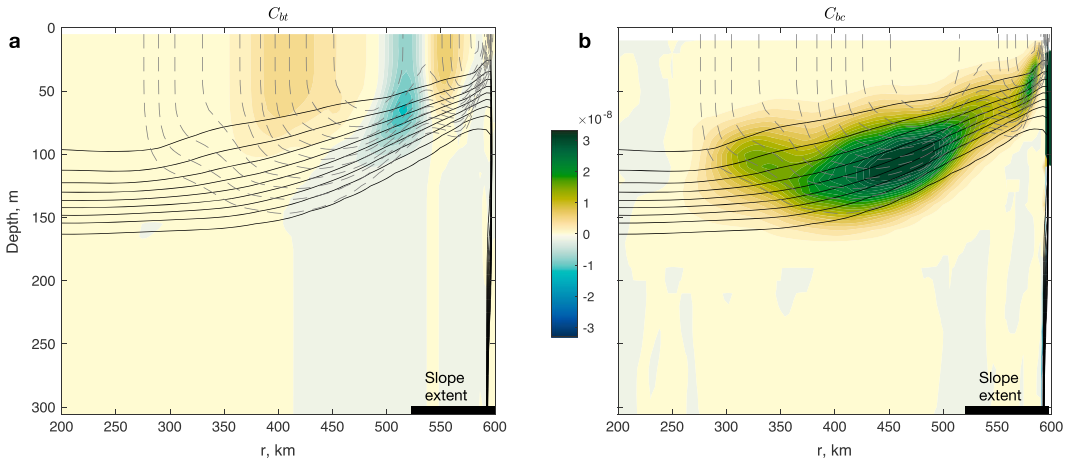

Figure 9. Energy conversion rates associated with eddy dynamics acting over (a) barotropic and (b) baroclinic mean flow shears for the control simulation with continental slope extending 75 km offshore. Solid curves display salinity contours spaced at 0.5, while the mean anticyclonic flow is shown with dashed gray contours equally spaced at 1 cm/s. Note the reduction of the baroclinic energy conversion rate over the slope.

associated kinetic energy can be dissipated. However, over the continental slope where the wind stress is the largest, baroclinic instability is suppressed and does not efficiently transfer momentum down. In these regions, barotropic instability transfers the wind-induced momentum offshore toward the flat-bottom regions where baroclinic instability can finally operate at full force.

Considering eddies as a direct stirring mechanism, it is somewhat counterintuitive that over continental slopes eddies generate strong momentum fluxes but weak buoyancy fluxes even though both gradients are strong there. This dynamical behavior arises because there is an additional constraint of vanishing residual mean stream function that leads to a three-way balance between the Ekman-driven, eddy momentum-driven and eddy thickness-driven stream functions. If the eddy thickness-driven stream function is weakened (due to topographic slope suppression of baroclinic instability), the eddy momentum-driven stream function must increase to compensate for this weakening—given the specified Ekman forcing. This dynamical behavior is qualitatively consistent with other idealized simulations of eddy dynamics over continental slopes under retrograde winds (Wang & Stewart, 2018).

6. Global Impacts of Reduced Eddy Diffusivities Over Continental Slopes

Here we use a simple analytical model of halocline depth evolution to highlight the mechanisms by which continental slopes, represented by a regional reduction of eddy diffusivity, affect the halocline equilibration timescale and FWC.

6.1. Time Evolution of Halocline Depth Near Its Equilibrium

Within the realms of the transient TEM framework, the halocline depth evolution is driven by three advection processes: Ekman pumping (w_{Ek}), a vertical velocity due to the eddy momentum-driven overturning cells (w_{em}), and a thickness-weighted eddy transport velocity (w^*). When the last vertical velocity is derived from an eddy thickness flux stream function and parameterized by the GM scheme, the resulting halocline depth evolution takes the form of a forced diffusion equation:

$$h_t = w_{\mathrm{Ek}} + w_{\mathrm{em}} + \frac{1}{r}\left(rKh_r\right)_r. \tag{10}$$

Here all dynamical variables are perturbations from their respective equilibrium means, and $K(r)$ is an eddy diffusivity for halocline perturbations that is defined by the characteristics of the mean state and is independent of time (Manucharyan et al., 2016).

The three vertical velocity contributions are equally important in determining the steady state gyre characteristics and when the residual overturning is near zero, there are strong compensations at play. So, as seen above, the time-mean w_{em} is strongly echoed in the form of the eddy diffusivity K that is substantially

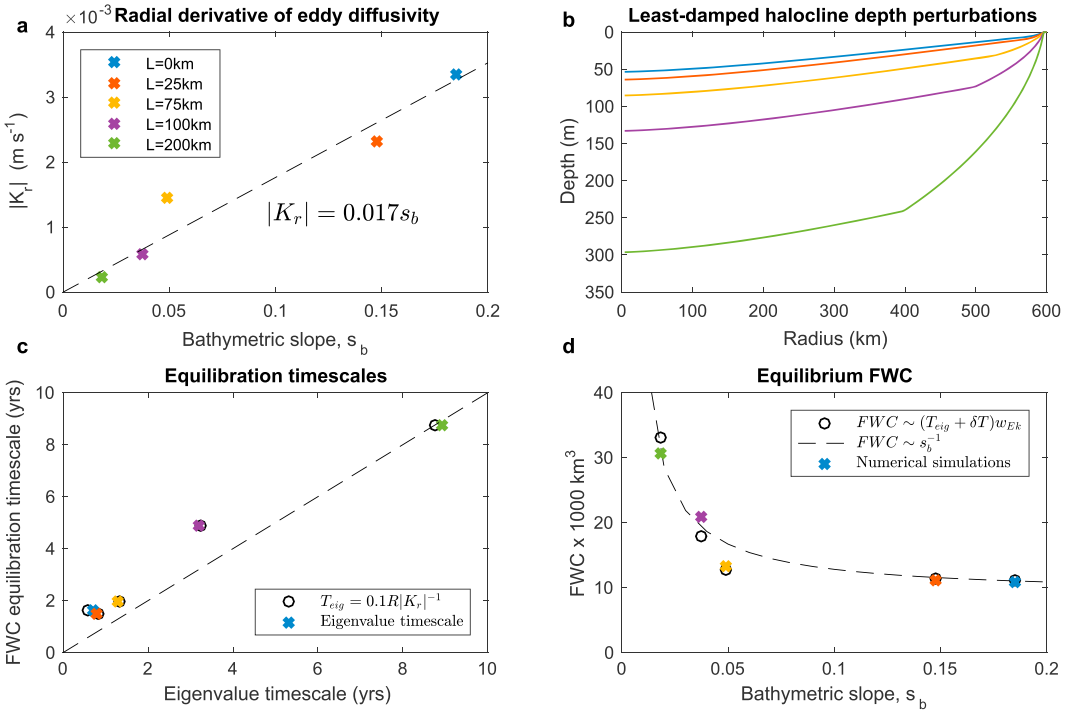

Figure 10. (a) Dependence of the near-wall radial derivative of eddy diffusivity, $|K_r|$, on the bathymetric slope, s_b. Dashed line denotes the best linear fit passing through (0, 0). (b) Least-damped halocline depth perturbations from the eigenvalue analysis (equation (10)), normalized to have their amplitude in the center of the gyre match the simulated equilibrium halocline depth. (c) Equilibration timescales obtained from the eigenvalue analysis (X axis) and estimated from the freshwater content (FWC) spin-up time series (Y axis) with dashed line denoting 1:1 ratio between the two. Circles represent an approximation of the eigenvalue timescales based on equation (12). (d) Equilibrium FWC plotted as a function of s_b as calculated from the adjusted eigenvalue timescales (circles), using a scaling law $FWC \sim s_b^{-1}$ (dashed line) and from numerical simulations (crosses). Colors are consistent across all panels. For the slope-free simulation, we used the deformation radius, R_d, to define the bathymetric slope as $s_b = H/R_d$ (instead of $s_b = H/L$) because dynamics with continental slopes extending to distances $L < R_d$ is indistinguishable from the slope-free dynamics.

reduced over continental slopes. However, contrary to Ekman-driven and eddy thickness transport, we do not yet have a clear way of parameterizing perturbations of w_{em}, which may depend on h and, in general, should not be treated as an external forcing. Nonetheless, in order to make progress here in identifying equilibration timescales, we make a simplification and disregard w_{em} in the layer thickness budget, focusing on the properties of the eddy thickness diffusion operator; we will justify this omission a posteriori.

In a halocline equilibrated by eddies, one could qualitatively think about the equilibration timescale as the time necessary for halocline perturbations to diffusively propagate across the entire gyre, from the points where boundary conditions are applied. The timescales are then inversely proportional to the magnitude of eddy diffusivity and hence are particularly sensitive to weak diffusivity regions that slow down the propagation of halocline depth perturbations. Note that regardless of whether continental slopes are present or not, the eddy diffusivity is expected to approach 0 in two places: in the center of the gyre because the halocline slope is 0 and at the coastal boundary because the eddies have no normal flow there (Figure 7). However, as we have seen, continental slopes extend the regions of locally weakened eddy diffusivity away from the coastal boundary. The result is that the rate of diffusivity increase with radius ($|K_r|$) is linearly proportional to the bathymetric slope, s_b (Figure 10a).

To quantify if the localized diffusivity weakening can indeed explain the observed behavior of gyre equilibration timescale and the equilibrium FWC (Figure 4), we solve the following eigenvalue problem:

$$\frac{1}{r}[rK(r)\tilde{h}_r]_r = -\frac{\tilde{h}}{T_{eq}}, \qquad \tilde{h}(R) = 0,\ \tilde{h}_r(0) = 0, \tag{11}$$

where $\tilde{h}(r)$ is the least-damped halocline eigenmode and T_{eq} is its equilibration timescale defined by the reciprocal of the corresponding eigenvalue (Manucharyan et al., 2016). The eigenvalues are calculated numerically and depend not only on the eddy diffusivity profile, $K(r)$, but also on the boundary conditions: a fixed halocline depth at the boundaries due to strong salinity restoring, $\tilde{h}(R) = 0$, and axial symmetry at the origin, $\tilde{h}_r(0) = 0$.

For the eigenvalue calculations, we take K profiles as diagnosed from the eddy-resolving numerical simulations shown in Figure 7b. Note, however, that the concept of diffusion via eddy stirring is only appropriate at length scales larger than a characteristic eddy scale. Hence, our spatially local definition of eddy diffusivity is not strictly appropriate in regions closer than an eddy length scale away from coastal boundaries. Nonetheless, it is clear that the eddy diffusivities at the boundaries must approach 0 because the no normal flow boundary condition implies a zero radial transport. Thus, in defining the eddy diffusivity over continental slopes (for $r > R - L$), we have imposed a linear diffusivity profile $K(r) = |K_r|(R - r)$ to ensure that it approaches 0 at the coastal boundaries. The characteristic radial derivative of the eddy diffusivity, $|K_r|$, is then defined by the local diffusivity value near the edge of the continental slope.

6.2. Equilibration Timescales and FWC From Eigenvalue Analysis

We focus on the properties of the gravest (least-damped) eigenmode that has the strongest projection onto FWC and dictates the equilibration timescale for the gyre (Manucharyan et al., 2016). The analysis, which is solely based on the diagnosed eddy diffusivity profiles, demonstrates that laterally extended continental slopes lead to amplified (deeper) halocline response to Ekman pumping perturbations and lengthened equilibration timescales (Figures 10b and 10c). The larger the extent of the weak diffusivity region, the deeper the least-damped halocline perturbations get and the stronger and more spread out the corresponding anticyclonic flow becomes. While the eigenvalue analysis describes the gyre response to perturbations near its equilibrium, the least-damped halocline perturbations show qualitative similarity with the equilibrium halocline shape (comparing Figures 3 and 10b). Furthermore, the eigenvalue timescales exhibit similar sensitivity to bathymetric slopes, being about $\delta T = 0.8$ years shorter compared to the observed FWC spin-up timescales (Figure 10c). The shorter eigenvalue timescales are expected as they are based on equilibrium eddy diffusivities while the gyre that is spun-up from rest takes additional time to fully develop the energetic eddy field; thus, δT accounts for the timescale associated with the development of baroclinic instabilities as well as for the eddy memory effect (Manucharyan et al., 2017). Nonetheless, the qualitative and also rather good quantitative agreement with the nonlinear spin-up simulations implies that the linear eigenvalue analysis does explain critical features of the gyre equilibration.

The eigenvalue analysis demonstrates that the systematic differences in the equilibration timescales and halocline depths are due to continental slopes significantly extending the region of weakened eddy diffusivity into the gyre interior. As it turns out, the equilibration timescales are only weakly sensitive to eddy diffusivities in the interior of the domain; when it comes to gyre equilibration, the bottleneck occurs over continental slopes where diffusivities increase from 0 at the gyre boundary to interior values at a linear rate, $|K_r|$ (Figures 7b and 10a). In fact, simply taking the diffusivity in the interior of the gyre to be much larger than over continental slopes leads to the eigenvalue timescale

$$T_{eig} \approx 0.1\, R\, |K_r|^{-1}, \tag{12}$$

and, as it turns out, this closely approximates the timescale calculated using the diagnosed diffusivity profile (compare crosses and circles in Figure 10c); the prefactor 0.1 has been calculated numerically by solving the nondimensional eigenvalue problem. Critically, T_{eig} depends on $|K_r|$ which, as we have seen, scales linearly with the bathymetric slope, that is, $|K_r| \sim s_b$ (Figure 10a). As a result, the equilibration timescale grows linearly with the lateral extent of continental slopes. Accounting for the lag between the nonlinear spin-up timescale and eigenvalue timescale, $T_{eq} = T_{eig} + \delta T$, and using equation (8) results in an accurate estimate of the equilibrium FWC (Figure 10d, circles), and further using equation (12), the FWC ends up being inversely proportional to the bathymetric slope: $FWC \sim s_b^{-1}$ (Figure 10d, dashed line). Note that a complete theory for T_{eq} and FWC still requires a clear eddy diffusivity parameterization as the constant of proportionality in the diagnosed empirical relation, $|K_r| \sim s_b$, is likely to be dependent on such dynamical parameters as stratification, bottom drag, and wind stress. This eddy parameterization issue must be addressed in further studies.

The reason that we were justified in discarding the contribution of the eddy momentum-driven overturning perturbations in the eigenvalue analysis becomes evident when we take note that the projection of $w_{em}(r,t)$ onto the least-damped halocline perturbation must be relatively small. The least-damped halocline perturbations are single-signed (Figure 10b), that is, having no zero crossings except at the boundary. In contrast, $w_{em}(r,t)$ emerging from two counterrotating cells changes its sign twice (Figure 8c), and hence, $\int w_{em}(r,t)\tilde{h}(r)\mathrm{d}r) \approx 0$. Instead, w_{em} projects strongly onto the second least-damped mode that decays about 4 times faster according to its eigenvalue. Any external forcing fields that project on higher eigenmodes does not significantly affect the FWC (see Figure 6 and corresponding discussion in Manucharyan et al., 2016). Thus, even if perturbations in w_{em} are of the same magnitude as the spatially uniform Ekman pumping perturbations, their impact on FWC perturbations is dramatically weaker and can be neglected. Note that the above eigenvalue results are strictly speaking limited to small-amplitude halocline perturbations. Therefore, accurately predicting the nonlinear gyre spin-up requires the development of parameterizations for the stream functions driven by both eddy momentum and thickness fluxes.

7. Summary and Discussion

This idealized model study demonstrates the critical influence of continental slopes on the dynamics of the BG of the Arctic Ocean. Consistent with existing theoretical ideas, when fields are integrated azimuthally around the gyre, there is an approximate balance between the Eulerian mean and eddy stream functions such that the residual overturning is small. However, the Eulerian mean overturning, conventionally assumed to depend only on Ekman pumping, is to leading order affected by eddy momentum fluxes, and over continental slopes the net Eulerian mean overturning is dramatically weakened. To create a small residual overturning, the eddy thickness flux overturning is also reduced over the slopes even if isopycnals are steepest there. Specifically, the eddy thickness diffusivity over the slopes is reduced by an order of magnitude compared to the slope-free gyre interior. The resulting mean state associated with extended continental slopes is characterized by a deeper halocline and a longer equilibration timescale compared to a slope-free gyre. Both of these gyre characteristics can be qualitatively explained by the reduced eddy thickness diffusivity over continental slopes.

It is instructive to point out that this basic Ekman and eddy-driven halocline dynamics is mathematically analogous to the problem of heat preservation in houses. The time evolution of temperature in a house and halocline depth in the gyre both obey a forced diffusion equation, and the inclusion of continental slopes is analogous to the inclusion of wall/roof insulation in the house as both reduce the diffusion coefficient. As a result of insulation, the equilibrated temperature is higher and the heat content in the house stays for a longer time, which directly corresponds to the increased FWC and prolonged equilibration timescale for the gyre with continental slopes.

We note that there are potential drawbacks associated with our idealized BG model configuration, mainly due to the omission of sea ice cover and the inclusion of salinity restoring at the boundaries. Since the ice-ocean drag depends on the difference between the ice and surface ocean velocity, the presence of sea ice affects (i) the magnitude of the average stress exerted on the ocean (and hence the Ekman pumping) and (ii) the energetics of the eddy field by providing a strong dissipation mechanism at the surface. Currently, the BG is seasonally ice covered, so with the continuing reduction of sea ice extent it seems likely that the ice-free eddy dynamics discussed here will become increasingly relevant. Nonetheless, we expect that the fundamental nature of eddy-slope dynamics will persist even when eddy energy levels are modulated by dissipation due to sea ice drag. Our other idealization of salinity restoring aims to represent the shelf-slope exchange of freshwater and pushes the gyre to a regime of infinite freshwater availability where only its internal dynamics determines the magnitude of equilibrated FWC. This regime is perhaps more relevant on longer timescales, while on shorter timescale, the gyre could behave more adiabatically where freshwater is only redistributed laterally and its total FWC is preserved. A gyre model that is most relevant to the observed BG perhaps consists of a mixture between these two limiting cases.

This is a preliminary study meant to bring attention to the issue of topographic effects on mesoscale eddy transport in the Arctic Ocean and in the BG in particular. Since the largest geostrophic currents and sharpest density and property fronts occur over continental slopes, it is crucial for low-resolution climate projection models to accurately parameterize eddy dynamics over these slopes. Currently, mesoscale eddy parameterization in Coupled Model Intercomparison Project class models do not include any continental slope

dependence and therefore likely introduce systematic errors in fluxes and large-scale fields. Our study shows that eddy diffusivities are the weakest over continental slopes despite having the steepest isopycnals slopes there. The topographically locked fronts are baroclinically unstable but not nearly as much as they would be over a flat bottom. So it is reasonable to believe that models typically overestimate exchanges between the Arctic Ocean boundary current and interior gyres, especially if they employ diffusivities that are merely proportional to isopycnal slopes (as proposed by, for example, Visbeck et al., 1997) The predictions by the modified Eady model of Blumsack and Gierasch (1972) are also unsatisfactory since this theoretical model ignores the crucial role of eddy momentum fluxes identified here for the $\delta > 1$ regime. Ultimately, a proper understanding and the development of parameterizations need to involve both components of the Eliassen-Palm flux, that is, on eddy PV fluxes. As suggested by the results found here, any projected BG responses to interannual or decadal wind variability obtained via low-resolution ocean models that keep employing traditional eddy parameterization schemes should be questioned.

Acknowledgments
All information necessary to reproduce the numerical experiments and data analysis is present in the paper and requires the use of publicly available software. G. E. M. acknowledges support from the Stanback Postdoctoral Fellowship at Caltech. P. E. I. was partially funded by grant 221780 (NorSEE) from the Research Council of Norway. This work used the Extreme Science and Engineering Discovery Environment (XSEDE; Towns et al., 2014), which is supported by NSF grant ACI-1053575. The manuscript benefited from discussions at the annual Forum for Arctic Modeling and Observing Synthesis (FAMOS) funded by the NSF OPP award PLR-1313614 and PLR-1203720. The authors thank John Marshall and an anonymous reviewer for their insightful comments.

References

Aksenov, Y., Ivanov, V. V., Nurser, A. G., Bacon, S., Polyakov, I. V., Coward, A. C., et al. (2011). The Arctic circumpolar boundary current. *Journal of Geophysical Research*, *116*, C09017. https://doi.org/10.1029/2010JC006637

Andrews, D. G., & McIntyre, M. E. (1976). Planetary waves in horizontal and vertical shear: The generalized eliassen-palm relation and the mean zonal acceleration. *Journal of the Atmospheric Sciences*, *33*(11), 2031–2048.

Armitage, T. W., Bacon, S., Ridout, A. L., Thomas, S. F., Aksenov, Y., & Wingham, D. J. (2016). Arctic sea surface height variability and change from satellite radar altimetry and GRACE, 2003–2014. *Journal of Geophysical Research: Oceans*, *121*, 4303–4322. https://doi.org/10.1002/2015JC011579

Beaufort Gyre Exploration Project (2019). WHOI Website, http://www.whoi.edu/page.do?pid=161756

Blumsack, S. L., & Gierasch, P. (1972). Mars: The effects of topography on baroclinic instability. *Journal of the Atmospheric Sciences*, *29*(6), 1081–1089.

Brink, K. (2012). Baroclinic instability of an idealized tidal mixing front. *Journal of Marine Research*, *70*(4), 661–688.

Dewey, S., Morison, J., Kwok, R., Dickinson, S., Morison, D., & Andersen, R. (2018). Arctic ice-ocean coupling and gyre equilibration observed with remote sensing. *Geophysical Research Letters*, *45*, 1499–1508. https://doi.org/10.1002/2017GL076229

Eady, E. T. (1949). Long waves and cyclone waves. *Tellus*, *1*(3), 33–52.

Eden, C., & Böning, C. (2002). Sources of eddy kinetic energy in the Labrador Sea. *Journal of Physical Oceanography*, *32*(12), 3346–3363.

Gent, P. R., & Mcwilliams, J. C. (1990). Isopycnal mixing in ocean circulation models. *Journal of Physical Oceanography*, *20*(1), 150–155.

Gent, P. R., Willebrand, J., McDougall, T. J., & McWilliams, J. C. (1995). Parameterizing eddy-induced tracer transports in ocean circulation models. *Journal of Physical Oceanography*, *25*(4), 463–474.

Giles, K. A., Laxon, S. W., Ridout, A. L., Wingham, D. J., & Bacon, S. (2012). Western Arctic Ocean freshwater storage increased by wind-driven spin-up of the Beaufort Gyre. *Nature Geoscience*, *5*(3), 194.

Haine, T. W., et al. (2015). Arctic freshwater export: Status, mechanisms, and prospects. *Global and Planetary Change*, *125*, 13–35.

Hoskins, B. J., James, I. N., & White, G. H. (1983). The shape, propagation and mean-flow interaction of large-scale weather systems. *Journal of the Atmospheric Sciences*, *40*(7), 1595–1612.

Isachsen, P. E. (2011). Baroclinic instability and eddy tracer transport across sloping bottom topography: How well does a modified eady model do in primitive equation simulations? *Ocean Modelling*, *39*(1-2), 183–199.

Johnson, H. L., Cornish, S. B., Kostov, Y., Beer, E., & Lique, C. (2018). Arctic ocean freshwater content and its decadal memory of sea-level pressure. *Geophysical Research Letters*, *45*, 4991–5001. https://doi.org/10.1029/2017GL076870

Lique, C., Johnson, H. L., & Davis, P. E. (2015). On the interplay between the circulation in the surface and the intermediate layers of the Arctic Ocean. *Journal of Physical Oceanography*, *45*(5), 1393–1409.

Luyten, J., Pedlosky, J., & Stommel, H. (1983). The ventilated thermocline. *Journal of Physical Oceanography*, *13*(2), 292–309.

Manucharyan, G. E., & Spall, M. A. (2016). Wind-driven freshwater buildup and release in the Beaufort Gyre constrained by mesoscale eddies. *Geophysical Research Letters*, *43*, 273–282. https://doi.org/10.1002/2015GL065957

Manucharyan, G. E., Spall, M. A., & Thompson, A. F. (2016). A theory of the wind-driven Beaufort Gyre variability. *Journal of Physical Oceanography*, *46*(11), 3263–3278.

Manucharyan, G. E., Thompson, A. F., & Spall, M. A. (2017). Eddy memory mode of multidecadal variability in residual-mean ocean circulations with application to the Beaufort Gyre. *Journal of Physical Oceanography*, *47*(4), 855–866.

Marshall, J., Adcroft, A., Hill, C., Perelman, L., & Heisey, C. (1997a). A finite-volume, incompressible Navier Stokes model for studies of the ocean on parallel computers. *Journal of Geophysical Research*, *102*(C3), 5753–5766.

Marshall, J., Hill, C., Perelman, L., & Adcroft, A. (1997b). Hydrostatic, quasi-hydrostatic, and nonhydrostatic ocean modeling. *Journal of Geophysical Research*, *102*(C3), 5733–5752.

Marshall, J., & Radko, T. (2003). Residual-mean solutions for the antarctic circumpolar current and its associated overturning circulation. *Journal of Physical Oceanography*, *33*(11), 2341–2354.

Marshall, J., Scott, J., & Proshutinsky, A. (2017). climate response functions for the arctic ocean: A proposed coordinated modelling experiment. *Geoscientific Model Development*, *10*(7), 2833–2848.

Mechoso, C. R. (1980). Baroclinic instability of flows along sloping boundaries. *Journal of the Atmospheric Sciences*, *37*(6), 1393–1399.

Meneghello, G., Marshall, J., & Campin, J.-M. (2018b). Negative feedbacks between wind, sea-ice and ocean currents damps the response of the Beaufort Gyre to changing winds. Ocean Sciences Meeting, 2018, Abstract.

Meneghello, G., Marshall, J., Cole, S. T., & Timmermans, M.-L. (2017). Observational inferences of lateral eddy diffusivity in the halocline of the Beaufort Gyre. *Geophysical Research Letters*, *44*, 12,331–12,338. https://doi.org/10.1002/2017GL075126

Meneghello, G., Marshall, J., Timmermans, M.-L., & Scott, J. (2018a). Observations of seasonal upwelling and downwelling in the Beaufort Sea mediated by sea ice. *Journal of Physical Oceanography*, *48*(4), 795–805.

Nurser, A., & Bacon, S. (2014). The Rossby radius in the Arctic Ocean. *Ocean Science*, *10*(6), 967–975.

Pedlosky, J. (1982). *Geophysical fluid dynamics* (636 p.). New York and Berlin: Springer-Verlag.
Phillips, N. A. (1954). Energy transformations and meridional circulations associated with simple baroclinic waves in a two-level, quasi-geostrophic model. *Tellus*, *6*(3), 274–286.
Plumb, R. A., & Ferrari, R. (2005). Transformed Eulerian-mean theory. Part I: Nonquasigeostrophic theory for eddies on a zonal-mean flow. *Journal of Physical Oceanography*, *35*(2), 165–174.
Proshutinsky, A., Bourke, R., & McLaughlin, F. (2002). The role of the Beaufort Gyre in Arctic climate variability: Seasonal to decadal climate scales. *Geophysical Research Letters*, *29*(23), 2100. https://doi.org/10.1029/2002GL015847
Proshutinsky, A., Krishfield, R., Timmermans, M.-L., Toole, J., Carmack, E., McLaughlin, F., et al. (2009). Beaufort Gyre freshwater reservoir: State and variability from observations. *Journal of Geophysical Research*, *114*, C00A10. https://doi.org/10.1029/2008JC005104
Schneider, T. (2006). The general circulation of the atmosphere. *Annual Review of Earth and Planetary Sciences*, *34*, 655–688.
Spall, M. A. (2013). On the circulation of Atlantic water in the Arctic Ocean. *Journal of Physical Oceanography*, *43*(11), 2352–2371.
Steele, M., Morley, R., & Ermold, W. (2001). PHC: A global ocean hydrography with a high-quality Arctic Ocean. *Journal of Climate*, *14*(9), 2079–2087.
Vallis, G. K. (2006). Atmospheric and Oceanic Fluid Dynamics. Atmospheric and Oceanic Fluid Dynamics, by Geoffrey K. Vallis (pp. 770). Cambridge University Press.
Visbeck, M., Marshall, J., Haine, T., & Spall, M. (1997). Specification of eddy transfer coefficients in coarse-resolution ocean circulation models. *Journal of Physical Oceanography*, *27*(3), 381–402.
Visbeck, M., Marshall, J., & Jones, H. (1996). Dynamics of isolated convective regions in the ocean. *Journal of Physical Oceanography*, *26*, 1721–1734.
Wang, Y., & Stewart, A. L. (2018). Eddy dynamics over continental slopes under retrograde winds: Insights from a model inter-comparison. *Ocean Modelling*, *121*, 1–18.
Wardle, R., & Marshall, J. (2000). Representation of eddies in primitive equation models by a PV flux. *Journal of Physical Oceanography*, *30*, 2481–2503.
Zhao, M., Timmermans, M.-L., Cole, S., Krishfield, R., & Toole, J. (2016). Evolution of the eddy field in the Arctic Ocean's Canada Basin, 2005–2015. *Geophysical Research Letters*, *43*, 8106–8114. https://doi.org/10.1002/2016GL069671
Zhao, M., Timmermans, M.-L., Krishfield, R., & Manucharyan, G. (2018). Partitioning of kinetic energy in the Arctic Ocean's Beaufort Gyre. *Journal of Geophysical Research: Oceans*, *123*, 4806–4819. https://doi.org/10.1029/2018JC014037
Zhong, W., Steele, M., Zhang, J., & Zhao, J. (2018). Greater role of geostrophic currents in ekman dynamics in the western Arctic Ocean as a mechanism for Beaufort Gyre stabilization. *Journal of Geophysical Research: Oceans*, *123*, 149–165. https://doi.org/10.1002/2017JC013282